Hindawi Publishing Corporation
Journal of Nanomaterials
Volume 2015, Article ID 321354, 7 pages
http://dx.doi.org/10.1155/2015/321354

Research Article

Direct Determination of Spatial Localization of Carriers in CdSe-CdS Quantum Dots

Yichen Zhao,[1] Abhilash Sugunan,[2] Qin Wang,[3] Xuran Yang,[1] David B. Rihtnesberg,[3] and Muhammet S. Toprak[1]

[1]*Department of Materials and Nano Physics, KTH Royal Institute of Technology, Kista, 16 440 Stockholm, Sweden*
[2]*Chemistry, Materials and Surfaces Unit, SP Technical Research Institute of Sweden, 114 86 Stockholm, Sweden*
[3]*Department of Sensor System, Acreo Swedish ICT AB, 16 440 Stockholm, Sweden*

Correspondence should be addressed to Abhilash Sugunan; abhilash.sugunan@sp.se and Muhammet S. Toprak; toprak@kth.se

Received 17 April 2015; Accepted 30 May 2015

Academic Editor: Ping Yang

Colloidal quantum dots (QDs) have gained significant attention due to their tunable band gap, simple solution processability, ease of scale-up, and low cost. By carefully choosing the materials, core-shell heterostructure QDs (HQDs) can be further synthesized with a controlled spatial spread of wave functions of the excited electrons and holes for various applications. Many investigations have been done to understand the exciton dynamics by optical characterizations. However, these spectroscopic data demonstrate that the spatial separation of the excitons cannot distinguish the distribution of excited electrons and holes. In this work, we report a simple and direct method to determine the localized holes and delocalized electrons in HQDs. The quasi-type-II CdSe-CdS core-shell QDs were synthesized via a thermolysis method. Poly(3-hexylthiophene) (P3HT) nanofiber and ZnO nanorods were selected as hole and electron conductor materials, respectively, and were combined with HQDs to form two different nanocomposites. Photoelectrical properties were evaluated under different environments via a quick and facile characterization method, confirming that the electrons in the HQDs were freely accessible at the surface of the nanocrystal, while the holes were confined within the CdSe core.

1. Introduction

Colloidal quantum dots (QDs) have attracted attention for several optoelectronic applications due to their tunable band gap, simple solution processability, ease of scale-up, and high reproducibility [1–4]. By carefully choosing the materials, core-shell heterostructure QDs (HQDs) can be further synthesized to have a staggered alignment of band edges. For instance, it was reported that type-I HQDs, such as CdSe-ZnS core-shell QDs, would trap the excitons within the CdSe core, leading to maximum fluorescence efficiency. These type-I HQDs find widespread applications in biodiagnostics, light emitting diodes, and so forth [5, 6]. On the other hand, the HQDs can also be designed to have a core-shell interface, where only excited electron or the hole encounters a potential barrier, named "quasi-type-II" QDs. Due to the significantly nonoverlapping wave functions of excited electron and hole in this type of HQDs, the exciton lifetime of the HQDs is long. For instance, it is widely reported that the excited electrons in CdSe-CdS HQDs are delocalized in the entire hetero-nanocrystal, due to a negligible conduction level offset between the CdSe core and CdS shell; meanwhile a large valence level offset confines the holes within the CdSe core [7, 8]. Taking the advantage of the spatial separation of excitons, the quasi-type-II HQDs were considered as a promising light absorbing candidate for photovoltaics.

Many works have been done to investigate the exciton dynamics in the HQDs via optical characterizations, such as transient absorption (TA) spectroscopic measurements and time-resolved photoluminescence (TRPL) spectroscopic measurements [9–11]. However, from these spectroscopic data, one can observe either the shift of absorption peak or the decay of the emission lifetime, which only helps to demonstrate the "relative" spatial separation of excitons rather than the actual spatial distribution of the excited electrons and holes within the heteronanocrystal. Surprisingly, there are

very few investigations reporting the direct methods which can directly determine the actual distribution of excitons in the HQDs. Finding out a solution to determine the spatial distribution of the hole/electron is useful for a better design of devices. By comparing the current response of HQDs together with the hole conductor and electron conductor, one can easily assess whether the holes are confined, or vice versa.

In this work, we report a facile characterization method to determine the spatial separation of excitons in HQDs, showing an unambiguous proof of the confinement of excited holes. We combined CdSe-CdS core-shell HQDs with P3HT to form HQD-P3HT nanocomposite. Poly(3-hexylthiophene) (P3HT) is a p-type conjugated polymer, which has been widely investigated as a hole conductor in many optoelectronic devices, owing to its high mobility [12]. The photoelectrical properties of the obtained HQD-P3HT nanocomposite were measured via *I-V* measurements. We found a "turn-on" behavior under low bias voltage in the current response curve, indicating the localization of the excited hole in the CdSe core. Meanwhile, when combined with ZnO nanorods, used as electron conductors, the current showed a fast increase in the low bias voltage with no indication of a "turn-on" voltage in the *I-V* measurements. Thus, we confirmed that the electrons from HQDs were freely accessible in the entire nanocrystal, while the holes were confined in the CdSe core. We believe that this is the first instance of a direct evaluation of the (de)localization of the carriers in quasi-type-II HQDs.

2. Materials and Methods

2.1. Materials. Cadmium oxide (CdO) (99.9%), selenium powder (99.9%), sulfur powder (99.9%), 1-octadecene (ODE) (90%), oleic acid (OA) (90%), n-hexane (90%), trioctylphosphine (TOP) (90%), zinc acetate dihydrate (98%), mercaptopropionic acid (MPA), and hexamethylenetetramine (hexamine) (99.5%) were purchased from Sigma-Aldrich. Zinc nitrate was purchased from Merck. All chemicals were used without further purification.

2.2. Synthesis of CdSe-CdS QDs

2.2.1. Stock Solution Preparation. Cd-oleate was prepared by heating the mixture solution of CdO powder with ODE and OA to 170°C for 2 h with N_2 flow. TOP-Se was made by mixing Se powder with ODE and TOP at 200°C for 2 h. TOP-S solution was prepared by mixing S powder with ODE and TOP at room temperature under N_2 atmosphere.

2.2.2. Synthesis of CdSe-CdS QDs. Cd-oleate was added to 4 mL of ODE and heated up to 220°C. 1 mL of TOP-Se was rapidly injected into the solution for 30 min to form CdSe core. 1 mL of the obtained core solution was added to 4 mL ODE and heated up to 300°C; Cd-oleate and TOP-S were injected dropwise in sequence. The injection process was repeated several times in order to grow a thick shell.

The final products were washed by ethanol and redispersed in hexane to form HQDs solution.

2.3. Synthesis of ZnO Nanorods

2.3.1. ZnO Seed Layer Preparation. 0.085 g zinc acetate was added to 8 mL ethanol and the solution was stirred until complete dissolution. 100 μL of the solution was then drop-casted on the precleaned glass substrate, which was then heated to 300°C for 30 min to form a thin layer of ZnO seed strongly adhered onto the substrate.

2.3.2. ZnO Nanorods Growth. Zinc nitrate and hexamine (molar ratio 1 : 1) were added to DI water in sequence and the solution was stirred until complete dissolution. The precursor solution was then transferred into a sealable container and the glass substrate with ZnO seed layer was placed inverted into the precursor solution. The container was then sealed and immersed into a glycerin bath at 85°C for 6-hour growth. Thereafter, the glass substrate was taken out and was gently rinsed in the deionized water to rinse away large precipitates. To optimize the process, three series of experiments were designed: (1) varying the precursor concentration from 10 mM to 100 mM, (2) varying the reaction time from 2 h to 14 h, and (3) varying reaction temperature from 65°C to 95°C.

2.4. Fabrication of the Nanocomposite

2.4.1. HQD-P3HT Nanocomposite. The HQDs solution was mixed with P3HT nanofiber solution, stirring for more than 24 hours under N_2 atmosphere until the HQDs were attached to P3HT nanofibers.

2.4.2. HQD-ZnO Nanocomposite. The ZnO nanorods substrate was first immersed into the HQDs solution for 5 seconds and then was lifted up gently for drying. Afterwards, the substrate was immersed into MPA solution for a few seconds and was lifted up for drying. This dip-coating route was repeated 3 times to ensure sufficient HQDs attached onto the ZnO nanorods.

2.5. Characterization. The absorption spectra of ZnO nanorods and their nanocomposite were obtained by using PerkinElmer's Lambda 750 UV/Vis spectrometer. Scanning Electron Microscopy (SEM) was done with a Zeiss Ultra 55 to confirm the different size of ZnO nanorods. Transmission Electron Microscopy (TEM) was done with a JEOL JEM-2100F operating at 200 kV to confirm the hybrid ZnO nanorod and QDs. The photoelectrical properties were evaluated under different environments: no illumination, visible light illumination (0.1 mW/cm^2), and UV illumination (360 nm; 0.5 mW/cm^2), by using Karl Suss PM5 and HP precision semiconductor parameter analyzer (Hewlett Packard 4156A).

3. Results and Discussion

3.1. Morphology and Optical Property of HQDs and HQD-P3HT Nanocomposite. The CdSe-CdS core-shell HQDs were synthesized via thermolysis method, using a similar route reported in our earlier work [13]. The obtained HQDs had a very thick CdS shell (>20 nm) overcoating a spherical CdSe

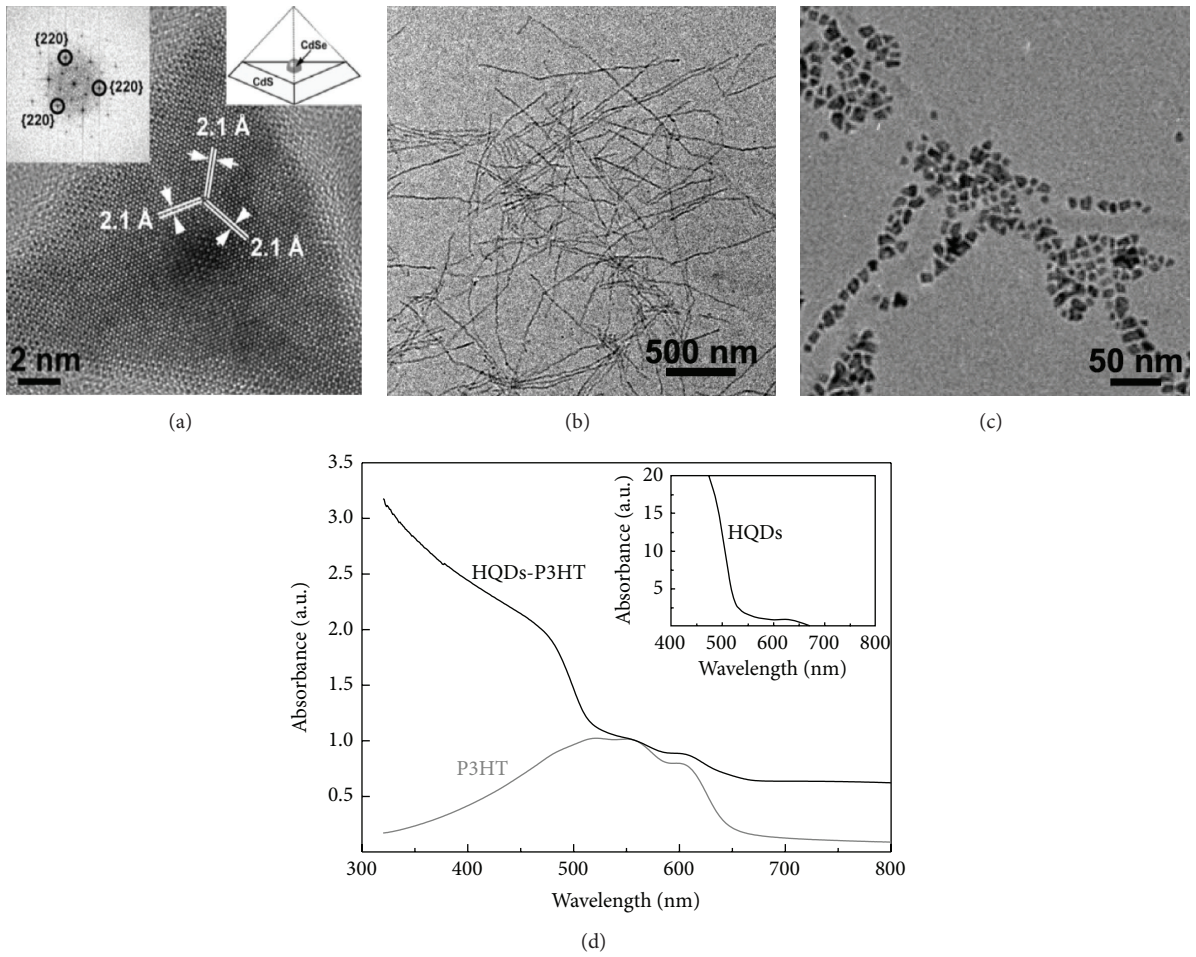

Figure 1: (a) TEM micrograph of CdSe-CdS HQDs (insets: indexed fast Fourier transform image and a schematic representation of the HQD). (b) TEM micrograph of P3HT nanofibers. (c) TEM micrograph of HQD-P3HT nanocomposite. (d) Absorption spectra of P3HT nanofibers and HQD-P3HT nanocomposite (insets: absorption spectra of HQDs).

core with diameter of ~4 nm. Due to a uniform crystal growth along the cubic {111} direction, the CdS shell showed a tetrahedral morphology, as shown in Figure 1(a). Our earlier study indicated the occurrence of spatial separation of excitons in the HQDs by a series of optical characterizations [13]. To further determine whether the holes are trapped within the CdSe core of these HQDs, the synthesized HQDs were combined with a solution of P3HT nanofibers to form a HQD-P3HT nanocomposite solution. We have reported a controlled synthesis of P3HT nanofiber via a modified whisker method. The highly crystalized P3HT nanofibers, with diameter of ~20 nm and length of ~2 μm, were obtained at room temperature, as shown in Figure 1(b) [13, 14]. P3HT was chosen because it is a well-known hole conducting material with superior conductivity when in the form of nanofibers [15]. The morphology of nanocomposite was analyzed by TEM and it was found that HQDs were well attached along the P3HT nanofibers (Figure 1(c)). The absorption spectra of pristine P3HT nanofibers as well as the HQD-P3HT nanocomposite were measured for comparison (Figure 1(d)). A significant difference of absorbance intensity was found between the two samples, especially in the UV range. For the pristine P3HT nanofibers, the absorbance intensity started to decrease after 500 nm. In contrast, an increase of absorbance intensity was observed after 500 nm for the HQD-P3HT nanocomposite, which is attributed to the presence of HQDs.

3.2. Photoelectrical Property of HQD-P3HT Nanocomposite. The obtained nanocomposite solution was drop-casted on an interdigitated electrode (IDE) with a spacing of 3 μm between electrodes. It was found that the IDE exhibited red luminescence under the UV light due to the presence of HQDs (Figure 2(a)). The *I-V* response across the electrodes was recorded under different environments, as shown in Figure 2(d). For comparison, similar *I-V* measurements with nanocomposite containing CdS single crystal QDs and pristine P3HT nanofibers were also performed (Figures 2(b) and 2(c)). Interestingly, we found that the current response of nanocomposite under all the three illumination conditions showed a distinct "turn-on" behavior. Furthermore, it was found that the "turn-on" voltage decreased with the energy of the illuminating light, lowest under UV illumination and highest under dark conditions. Nevertheless, these *I-V*

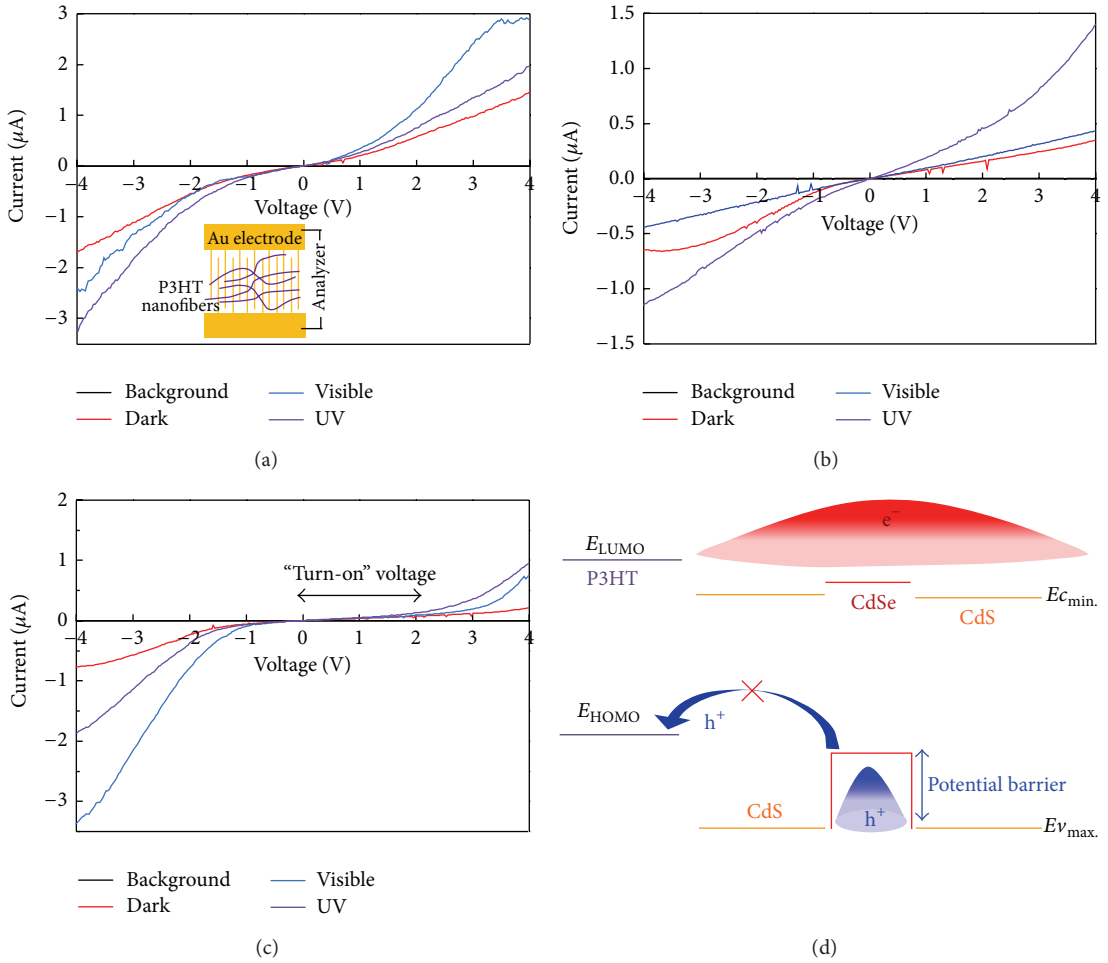

FIGURE 2: *I-V* response curves of (a) pristine P3HT nanofibers (insets: schematic diagram of Au electrode), (b) CdS-P3HT nanocomposite, and (c) HQD-P3HT nanocomposite. (d) Schematic potential diagram showing the alignment of the energy levels of the HQD-P3HT nanocomposite.

curves suggested that until a sufficient threshold voltage is provided there is negligible current flow. P3HT is a hole-conductor polymer; this *I-V* response indicated that under low bias voltage very few holes from the HQDs could reach P3HT nanofibers (Figure 2(d)). We therefore assumed that holes generated from the HQDs were initially trapped in the CdSe core and very few holes could be conducted out by P3HT. Only under a sufficient high bias voltage could the holes overcome the potential barrier at the core-shell interface and pass through the shell. Eventually, the released holes reached P3HT nanofibers, resulting in a sharp increase in measured current. For pristine P3HT nanofibers, visible light illumination resulted in the highest current, while in the case of nanocomposite with CdS QDs, UV illumination resulted in the highest measured current levels due to the existence of CdS QDs. However, in both of the reference cases, there was no observation of a similar "turn-on" voltage, which confirmed the confinement of holes in the HQDs.

3.3. Morphology and Optical Property of HQD-ZnO Nanocomposite. To further demonstrate the availability of the excited electrons on the surface of the HQDs, the HQDs were combined with ZnO nanorods to form HQD-ZnO nanocomposite. Unlike the case of HQD-P3HT nanocomposite, we expected that the electrons would be delocalized in the whole HQDs and could be conducted out easily. ZnO was chosen since it is a well-known electron conductor material, owing to its wide band gap [15, 16]. ZnO nanorods were synthesized via a chemical bath deposition [17, 18]. Different parameters, such as precursor concentrations, reaction time, and reaction temperature, were systematically investigated to optimize the synthesis process. It is found that, with the increasing concentration of precursors, the average diameter of final ZnO nanorods increased, while the average length of nanorod decreased. This could be attributed to a faster growth on lateral direction under a higher precursor concentration environment, leading to thicker but shorter nanorods. Meanwhile, the nanorods become more aligned on the substrate with the prolonged time and average length of nanorods increased with prolonged time. In addition, it is confirmed that the average diameter of ZnO nanorods dramatically increased once the temperature increased from 65°C to 75°C, while there was negligible increase in diameter from 75°C to

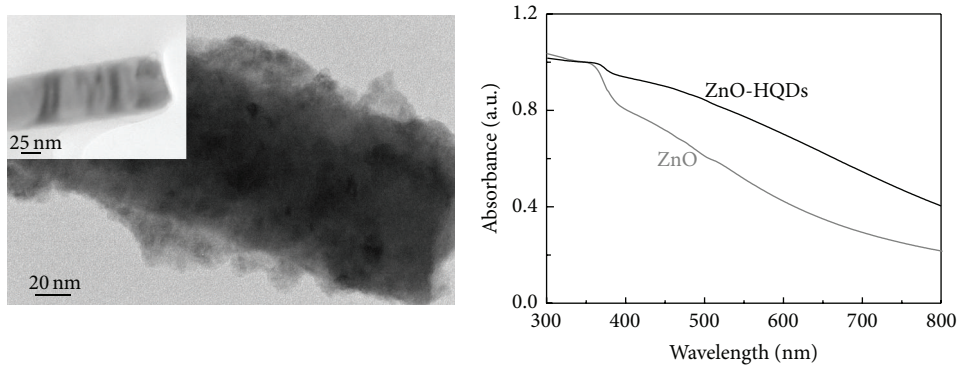

FIGURE 3: (a) TEM micrograph of ZnO-HQDs nanocomposite (inset: TEM micrograph of an uncoated ZnO nanorod as a comparison). (b) Absorption spectra of ZnO nanorods and ZnO-HQDs nanocomposite.

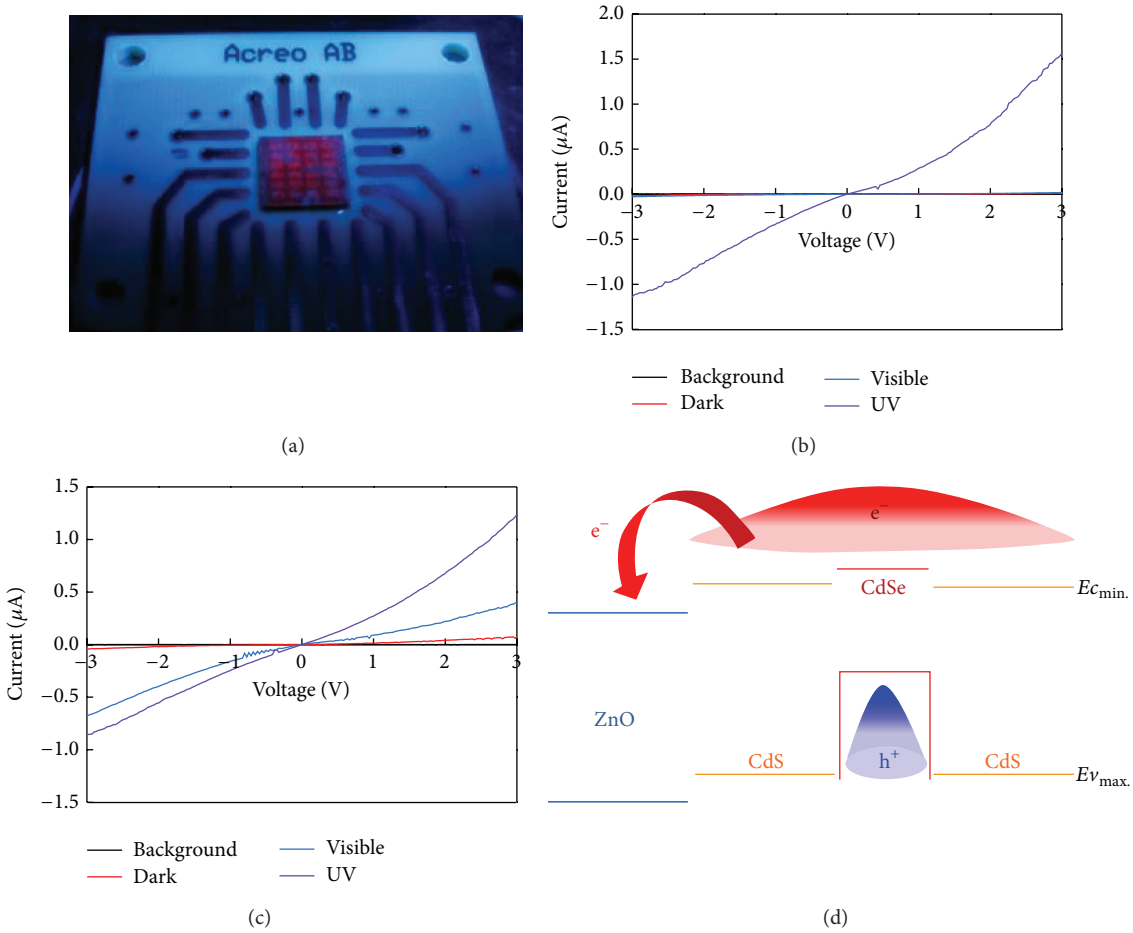

FIGURE 4: (a) HQD-ZnO nanocomposite drop-casted on the IDE under UV illumination and I-V response curve of (b) pristine ZnO nanorod and (c) HQD-ZnO nanocomposite. (d) Schematic potential diagram showing the alignment of energy levels of the HQD-ZnO nanocomposite.

95°C. Hence, we conclude that the critical temperature for sustaining the growth is 65°C and the size of ZnO nanorods is not affected once the temperature was above 75°C. The obtained ZnO nanorods from the optimized process were thereafter combined with HQDs via surface modification, forming HQD-ZnO nanocomposite. The morphology of nanocomposite was analyzed by SEM, confirming that a uniform layer of HQDs is coated on the surface of ZnO nanorods (Figure 3(a)). The absorption spectra of HQD-ZnO nanocomposite as well as pristine ZnO were measured

(Figure 3(b)). Compared to the absorption spectrum of pristine ZnO nanorods, the absorbance intensity of HQD-ZnO nanocomposite increases remarkably, attributed to the presence of HQDs.

3.4. Photoelectrical Properties of HQD-ZnO Nanocomposite. The *I-V* response of HQD-ZnO nanocomposite was also evaluated by using similar IDE and conditions (Figure 4). It was found that the IDE exhibited red luminescence under the UV light due to the presence of HQDs (Figure 4(a)). For comparison, the *I-V* measurements with pristine ZnO nanorods were also performed (Figure 4(b)). For the pristine ZnO nanorod, a noticeable current response is observed only under UV illumination, which is consistent with the band gap energy of ZnO. However, compared to the reference sample, photocurrent intensity of HQD-ZnO nanocomposite increased 20 times under visible illumination (Figure 4(c)). Moreover, there was no "turn-on" behavior observed in all the current response curves. This absence of the "turn-on" voltage indicates that under visible illumination the excited electrons originated within the HQDs are freely available at the surface of CdS shell and then are easily ejected into the ZnO nanorod, resulting in an increase of current flow even at low bias voltages (Figure 4(d)).

4. Conclusion

In conclusion, CdSe-CdS HQDs were synthesized and further combined with the P3HT nanofibers and ZnO nanorods to form the HQD-P3HT and HQD-ZnO nanocomposites. Under the low bias voltage, a "turn-on" voltage behavior was found in the HQD-P3HT nanocomposite, indicating the confinement of excited holes in the CdSe core. Meanwhile, a direct increase of current response was found in the HQD-ZnO nanocomposite, showing delocalization of electrons in the entire CdSe-CdS HQDs. This is the first time such direct evaluation of the spatial separation of charges is being reported, providing concrete evidence on the carrier localization, which has great potential to design the optoelectronic devices in a better way.

Conflict of Interests

The authors declare that there is no conflict of interests regarding the publication of this paper.

Acknowledgments

The authors acknowledge the financial support from the Swedish Foundation for Strategic Research (SSF, Grant no. EM11-0002) and Swedish Research Council (VR-SRL 2013-6780).

References

[1] H. Wei, J. Zhou, L. Zhang, F. Wang, J. Wang, and C. Jin, "The core/shell structure of CdSe/ZnS quantum dots characterized by X-ray absorption fine spectroscopy," *Journal of Nanomaterials*. In press.

[2] A. P. Alivisatos, "Semiconductor clusters, nanocrystals, and quantum dots," *Science*, vol. 271, no. 5251, pp. 933–937, 1996.

[3] V. I. Klimov, A. A. Mikhailovsky, S. Xu et al., "Optical gain and stimulated emission in nanocrystal quantum dots," *Science*, vol. 290, no. 5490, pp. 314–317, 2000.

[4] H. Song and S. Lee, "Red light emitting solid state hybrid quantum dot-near-UV GaN LED devices," *Nanotechnology*, vol. 18, no. 25, Article ID 255202, 2007.

[5] T. Xuan, J. Liu, R. Xie, H. Li, and Z. Sun, "Microwave-assisted synthesis of CdS/ZnS:Cu quantum dots for white light-emitting diodes with high color rendition," *Chemistry of Materials*, vol. 27, no. 4, pp. 1187–1193, 2015.

[6] S.-W. Lee, J.-S. Kim, J.-S. Lee et al., "Enhancement of CdSe/ZnS quantum dot-based LED by core-shell modification," *Journal of the Korean Physical Society*, vol. 66, no. 1, pp. 82–86, 2015.

[7] H. Li, Q. Zhang, S. Zhou, and Q. Li, "Toward highly efficient CdS/CdSe quantum dot-sensitized solar cells incorporating a fullerene hybrid-nanostructure counter electrode on transparent conductive substrates," *RSC Advances*, vol. 5, no. 39, pp. 30617–30623, 2015.

[8] M. Saba, S. Minniberger, F. Quochi et al., "Exciton-exciton interaction and optical cain in colloidal CdSe/CdS Dot/Rod nanocrystals," *Advanced Materials*, vol. 21, no. 48, pp. 4942–4946, 2009.

[9] B. C. Fitzmorris, J. K. Cooper, J. Edberg, S. Gul, J. Guo, and J. Z. Zhang, "Synthesis and structural, optical, and dynamic properties of core/shell/shell CdSe/ZnSe/ZnS quantum dots," *Journal of Physical Chemistry C*, vol. 116, no. 47, pp. 25065–25073, 2012.

[10] T. Debnath, P. Maity, and H. N. Ghosh, "Super sensitization: grand charge (hole/electron) separation in ATC dye sensitized CdSe, CdSe/ZnS type-I, and CdSe/CdTe type-II core-shell quantum dots," *Chemistry—A European Journal*, vol. 20, no. 41, pp. 13305–13313, 2014.

[11] H. Zhu, Z. Chen, K. Wu, and T. Lian, "Wavelength dependent efficient photoreduction of redox mediators using type II ZnSe/CdS nanorod heterostructures," *Chemical Science*, vol. 5, no. 10, pp. 3905–3914, 2014.

[12] K. Schmoltner, F. Schlütter, M. Kivala et al., "A heterotriangulene polymer for air-stable organic field-effect transistors," *Polymer Chemistry*, vol. 4, no. 20, pp. 5337–5344, 2013.

[13] A. Sugunan, Y. Zhao, S. Mitra et al., "Synthesis of tetrahedral quasi-type-II CdSe-CdS core-shell quantum dots," *Nanotechnology*, vol. 22, no. 42, Article ID 425202, 2011.

[14] Y. Zhao, A. Sugunan, D. B. Rihtnesberg, Q. Wang, M. S. Toprak, and M. Muhammed, "Size-tuneable synthesis of photoconducting poly-(3-hexylthiophene) nanofibres and nanocomposites," *Physica Status Solidi C*, vol. 9, no. 7, pp. 1546–1550, 2012.

[15] S. Günes, H. Neugebauer, and N. S. Sariciftci, "Conjugated polymer-based organic solar cells," *Chemical Reviews*, vol. 107, no. 4, pp. 1324–1338, 2007.

[16] D. B. Rihtnesberg, S. Almqvist, Q. Wang et al., "ZnO nanorods/nanoflowers and their applications," in *Proceedings of the 4th IEEE International Nanoelectronics Conference (INEC '11)*, pp. 5–6, June 2011.

[17] X. Yang, *Synthesis of hybrid ZnO Nanowires-Quantum dots and their photoelectrical characterization [M.S. thesis]*, KTH-Royal Institute of Technology, 2010.

[18] D. B. Rihtnesberg, *Investigation of ZnO nanorods for UV detection [M.S. thesis]*, KTH—Royal Institute of Technology, 2011.